Journal of Photochemistry and Photobiology A: Chemistry 208 (2009) 131–140

Contents lists available at ScienceDirect

Journal of Photochemistry and Photobiology A: Chemistry

journal homepage: www.elsevier.com/locate/jphotochem

Spectral and photophysical properties of fluorone dyes in bio-related films and methanol

E. Slyusareva[a,*], A. Sizykh[a], A. Tyagi[b], A. Penzkofer[b]

[a] Siberian Federal University, Svobodny Prospect, 79, 660041 Krasnoyarsk, Russia
[b] Institut II – Experimentelle und Angewandte Physik, Universität Regensburg, Universitätsstrasse 31, D-93053 Regensburg, Germany

ARTICLE INFO

Article history:
Received 3 June 2009
Received in revised form 26 August 2009
Accepted 4 September 2009
Available online 10 September 2009

PACS:
83.80.Rs
33.50.–j

Keywords:
Fluorone dyes
Fluorescein
Dibromofluorescein
Eosin Y
Erythrosine B
Rose bengal
Biofilms
Gelatin
Starch
Chitosan
Absorption cross-sections
Luminescence quantum distributions
Fluorescence lifetimes
Phosphorescence

ABSTRACT

The fluorone dyes fluorescein, 4,5-dibromofluorescein, eosin Y, erythrosine B, and rose bengal in the biological materials gelatin, starch, and chitosan have been characterized by absorption and emission spectroscopy. Comparative studies were carried out for the same dyes in methanol. The absorption cross-section spectra, luminescence quantum distributions, luminescence quantum yields, fluorescence quantum yields, and degrees of luminescence polarization were determined by steady-state spectroscopy. The fluorescence lifetimes were measured by time-resolved laser experiments. High fluorescence quantum yields were obtained for fluorescein in both the solid hosts and the liquid solutions. The fluorescence reduction due to enhancement of intersystem crossing by heavy atom spin-orbit coupling was efficient both in the biofilms and in methanol. Room temperature phosphorescence emission was observed for the heavy atom substituted fluorescein derivatives in the biofilms. The spectroscopic behavior of the fluorone dyes depends on their ionic state with highest luminescence efficiency for the dianionic forms. This form was realized for all investigated dyes in basic methanol and in most cases also in the biofilms.

1. Introduction

Fluorone dyes are hydroxyl-xanthene dyes (homologues of fluorescein). From this group disodium fluorescein, 4,5-dibromofluorescein, disodium-2,4,5,7-tetrabromofluorescein (eosin Y), disodium-2,4,5,7-tetraiodofluorescein (erythrosine B), and disodium-3′,4′,5′,6′-tetrachloro-2,4,5,7-tetraiodofluorescein (rose bengal) in biofilms and methanol are spectroscopically characterized here. The structural formulae are displayed in Fig. 1.

Disodium fluorescein (Uranin) and 2,7-dichlorofluorescein (Fluorescein 27, Fluorescein 548) are widely used laser dyes [1–3]. Eosin Y was also applied as laser dye [3]. Fluorone dye polymeric films are used as media for optical recording of information [4]. Fluorescein and reactive derivatives of fluorescein have been the most widely used class of organic fluorophores for labeling and sensing biomolecules [5–8] because of their high absorption cross-sections, high fluorescence quantum yields, and their ability to attach to biomolecules. Fluorescein isothiocyanate is applied to protein (antibody or antigen) labeling [5–9]. Fluorescein derivatives are used as fluorescent probes for zinc in enzymes [8]. Fluorescent chitosan bearing fluorescein was synthesized as potential biomaterial for temperature probes and pH probes [10]. Fluorescein derivatives were synthesized for the construction of fluorescent reporters of protein kinase activity [11]. Fluorescein is applied as reference standard in quantum yield measurement [12]. Eosin was used as ligand for studying of bovine serum albumin (BSA) properties during denaturation–renaturation by fluorescence analysis [13]. Eosin Y was applied for free radical photopolymersiation of thin hydrogels in contact with arterial tissue [14]. Erythrosine was used as phosphorescent probe to detect the oxygen content dissolved in

* Corresponding author at: Institute of Engineering Physics, Siberian Federal University, Department of Experimental and Medical Physics, Prospect Svobodnyi, 79, 660041 Krasnoyarsk, Russia. Tel.: +7 391 244 54 69; fax: +7 391 244 86 25.
E-mail addresses: grad@lan.krasu.ru, 2_98_54_46@mail.ru (E. Slyusareva).

1010-6030/$ – see front matter © 2009 Elsevier B.V. All rights reserved.
doi:10.1016/j.jphotochem.2009.09.006

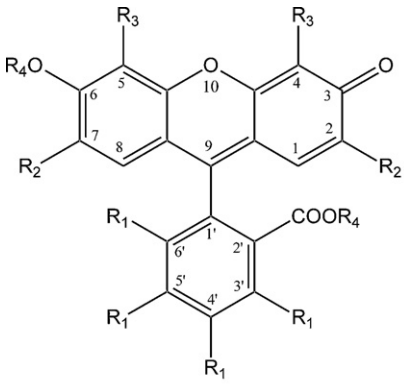

	R_1	R_2	R_3	R_4
Fluorescein	H	H	H	Na
Dibromofluorescein	H	H	Br	H
Eosin Y	H	Br	Br	Na
Erythrosine B	H	I	I	Na
Rose bengal	Cl	I	I	Na

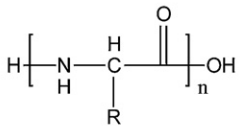

Gelatin (R: 27 % glycine, 16 % proline, 14 % oxyproline, 9 % arginine, 5 % lysine)

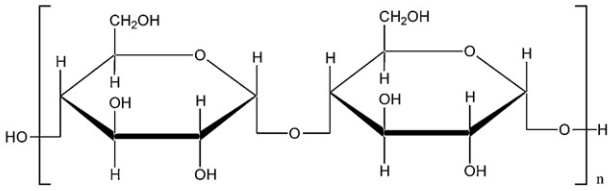

Starch

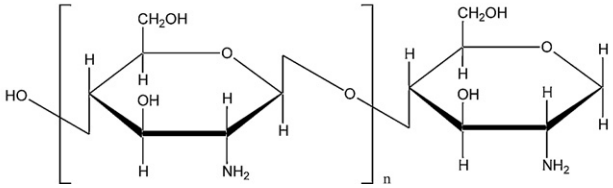

Chitosan

Fig. 1. Structural formulae of applied fluorone dyes and biopolymers.

sol–gel silica within a wide range of temperatures and pressures [15]. The photo-bleaching kinetics of eosin in gelatin was studied to clarify the involved photochemical mechanisms and to determine diffusion constants of the dye in the polymer [16,17]. Eosin doped gelatin films were applied to determine the spatial coherence and the cross-sectional intensity distribution of argon laser beams [18].

Progress in molecular photonics depends on achievements in fundamental studies of photophysical and photochemical parameters of fluorophores. Dyes with heavy atoms substituting hydrogen play a specific role. Substitutions allow redistributing the rates of radiative and non-radiative transitions in the molecules.

In an early paper Martin [19] showed that a red-shift in the absorption and fluorescence spectra of fluorescein and 6-hydroxy-9-phenyl-fluorone in alkaline solutions was caused by intermolecular hydrogen bonding with the solvent. The dye–solvent interaction turned out to cause a reduction of the fluorescence quantum yield and a growth of internal conversion probability. Fleming and co-authors [20] used picosecond spectroscopy to determine the rate constants of non-radiative transitions. The rate constant of intersystem crossing increased in the series fluorescein, eosin, rose bengal, erythrosine due to increasing spin-orbit coupling caused by the heavy atoms. A reduction of the S_1–T_1 energy gap and an increase of the S_0–S_1 energy gap were revealed in the sequence of solvents: iso-propanol, ethanol, methanol, H_2O.

Joshi et al. [21,22] studied the fluorescence and phosphorescence behavior of fluorescein, 2,7-dichlorofluorescein, 2,7-dibromofluorescein, triiodofluorescein (iodine atoms are substitutes of hydrogen atoms on carboxy-benzene group), and eosin. Dyes in the dianionic and cationic forms were examined. It was shown that an increase in mass of the substituting atoms does not change the radiative S_1–S_0 rate constant, but increases the rate constants of excited singlet–triplet intersystem crossing, phosphorescence, and non-radiative triplet state deactivation. Changes of rate constants were found to be more significant for cations than for anions [21]. All the examined dyes revealed the ability to aggregate. The influence of aggregation on the photophysical rate constants of eosin and erythrosine was shown in [22]. The rate constant of intersystem crossing reduced a factor of 10–100 by increasing the dye concentration from 5×10^{-5} to 10^{-1} M.

In [23] triplet–triplet absorption spectra of eosin Y, erythrosine B and rose bengal in methanol were determined in the wavelength region from 390 to 1600 nm. Photophysical parameters of these dyes were presented in [23–25].

Room temperature phosphorescence and delayed fluorescence of solid solutions of eosin and erythrosine in silica-gel glasses, boric acid glass and gelatin were studied in [26]. Using results of time-resolved measurements, the authors calculated rate constants of photophysical processes. Immobilization of halogen substituted fluorescein in polymer matrices (nitrocellulose and polyvinyl alcohol) allowed the detection of room temperature phosphorescence and delayed fluorescence in [27]. The orientation of the phosphorescent dipole moments of erythrosine B, 4,5-dibromofluorescein, 4,5-diiodofluorescein, and eosin Y immobilized in various polymer matrices was determined by time-resolved phosphorescence anisotropy measurements [27]. Phosphorescence and delayed flu-

orescence of eosin [28] and erythrosine [28,29] in de-aerated aqueous solution at room temperature was observed by laser flash spectroscopy.

Low-power phase-conjugation by degenerate four-wave mixing (transient grating formation) was achieved in thin films of eosin and erythrosine doped gelatin films in [30] by triplet state population. Similar results were obtained for fluorescein doped boric acid glass in [31,32].

Bio-related films have a wide field of applications in biology, cosmetology, and pharmaceutics because of their easy manufacturability, bio-compatibility, ecological compatibility, and their non-toxicity [33,34]. Chitosan scaffolds appear to be suitable for tissue engineering applications [35,36]. Gelatin and starch are used for immobilization of bioluminescence assays [37].

In this paper the spectral and photophysical properties of the above mentioned five fluorone dyes disodium-fluorescein (shortly called fluorescein), dibromofluorescein, eosin Y, erythrosine B, and rose bengal in bio-related films (gelatin, starch, chitosan) are studied to get fundamental optical information for their potential application in bio-photonics and bio-sensorics. Spectral and photophysical studies of the dyes in methanol were carried out for comparative purpose.

2. Materials and methods

2.1. Sample preparation

The disodium salts of rose bengal ($C_{20}H_2I_4Cl_4O_5Na_2$, molar mass $M = 1017.65\,g\,mol^{-1}$), erythrosine B ($C_{20}H_6I_4O_5Na_2$, $M = 879.86\,g\,mol^{-1}$), eosin Y ($C_{20}H_6O_5Br_4Na_2$, $M = 691.86\,g\,mol^{-1}$) and uranin (disodium fluorescein) ($C_{20}H_{10}O_5Na_2$, $M = 355.31\,g\,mol^{-1}$) were supplied by Sigma. The dye 4,5-dibromofluorescein ($C_{20}H_{10}Br_2O_5$, $M = 490.10\,g\,mol^{-1}$) was bought from Fluka. As biopolymers were used: photographic gelatin, grade A, from VEKTON; starch, soluble research grade from SERVA; and chitosan (polyaminosaccharide, 2-amino-2-deoxy-β-D-glucan), low-viscous, from Fluka. The structural formulae of the used biopolymers are included in Fig. 1. All chemicals were used as delivered.

Fluorone dye doped films of approximately 10 μm thickness were prepared by dissolving the dyes in neutral methanol and the biopolymers in Millipore water, then mixing them together, and slowly drying the solutions on glass substrates. The aqueous starch solutions were heated up to 80–85 °C, and then in cooling down the dyes in neutral methanol solution were added in order to obtain transparent films. The dye concentration in the films was in the range of 3×10^{-3} to 9×10^{-3} mol dm^{-3}. For comparison the fluorone dyes in basic methanol containing 0.1 mM NaOH were studied (dye concentration in the range of 8×10^{-5} to 2×10^{-4} M). Some studies were also carried out in neutral methanol and in acidic methanol (content of 10^{-4} M HCl). If not stated different then the short writing of methanol in this paper means methanol containing 10^{-4} M NaOH.

2.2. Spectroscopic techniques

Absorption cross-section spectra, $\sigma_a(\lambda)$, of the samples were determined by transmission measurements, $T(\lambda)$, with a commercial spectrophotometer (Cary 50 from Varian). The parameters are related by $T(\lambda) = \exp[-\alpha(\lambda)\ell] = \exp[-N_0\sigma_a(\lambda)\ell]$, where α is the absorption coefficient, ℓ is the sample length, and N_0 is the dye number density. For the dye doped films the determination of the dye concentration, $C = N_0/N_A$ (N_A is Avogadro constant), and the film thickness turned out to be inaccurate. Therefore $\sigma_a(\lambda)$ was extracted from $T(\lambda)$ and the radiative lifetime, τ_{rad}, which was determined by fluorescence lifetime, τ_F, and fluorescence quantum yield, ϕ_F, measurements ($\tau_{rad} = \tau_F/\phi_F$). The applied relations are

$$\sigma_a(\lambda) = -(N_0\ell)^{-1}\ln[T(\lambda)], \tag{1a}$$

with

$$(N_0\ell)^{-1} = -\frac{\int_{S_0-S_1}\frac{\sigma_a(\lambda)}{\lambda}\,d\lambda}{\int_{S_0-S_1}\frac{\ln[T(\lambda)]}{\lambda}\,d\lambda}. \tag{1b}$$

and

$$\int_{S_0-S_1}\frac{\sigma_a(\lambda)}{\lambda}\,d\lambda = \frac{n_A}{8\pi c_0 n_F^3\tau_{rad}}\frac{\int_{em}E_F(\lambda)\lambda^3\,d\lambda}{\int_{em}E_F(\lambda)\,d\lambda}. \tag{1c}$$

The last equation is the Strickler–Berg formula in a rewritten form [38–40]. n_A and n_F are the average refractive indices in the S_0–S_1 absorption region and in the S_1–S_0 emission region (em), respectively. c_0 is the speed of light in vacuum, and $E_F(\lambda)$ is the fluorescence quantum distribution. Luminescence spectra, $S_L(\lambda)$, were measured with a self-assembled spectrofluorimeter [41,42]. The samples were excited with a tungsten lamp combined with appropriate interference filters. The excitation light was polarized to the vertical with a thin film polarizer. A front-face arrangement was used for luminescence light collection (luminescence gathering in backward direction). For the liquid solutions cells of 1 mm thickness were used. The collimated luminescence light was focused to the entrance slit of a grating spectrometer and detected with a silicon diode-array detection system (TN-1710 multichannel analyzer with diode-array rapid scan spectrometer system from Tracor Northern). The luminescence spectra were corrected for the spectral sensitivity of the detection system. Orientation independent luminescence detection was achieved with a thin film polarizer in the detection path under magic angle direction (54.7° orientation to the vertical).

The intrinsic luminescence quantum distribution [43], $E_L(\lambda)$, was calculated from the measured luminescence spectra, $S_L(\lambda)$, by absolute calibration with rhodamine 6 G in methanol (fluorescence quantum yield $\phi_F = 0.94$ [44]) as reference standard. In the calculation of the fluorescence quantum distributions, the fluorescence reabsorption was corrected for by the applied analysis [41,42]. The intrinsic luminescence quantum yield was calculated by integration over the intrinsic luminescence quantum distribution, i.e. $\phi_L = \int E_L(\lambda)\,d\lambda$.

The degree of luminescence polarization,

$$P_L = \frac{\int S_{L,||}(\lambda)\,d\lambda - \int S_{L,\perp}(\lambda)\,d\lambda}{\int S_{L,||}(\lambda)\,d\lambda + \int S_{L,\perp}(\lambda)\,d\lambda} \tag{2}$$

was determined by measuring the luminescence spectra polarized parallel to the excitation light [$S_{L,||}(\lambda)$] and perpendicular to the excitation light [$S_{L\perp}(\lambda)$]. $S_{L,||}(\lambda)$ and $S_{L\perp}(\lambda)$ were also corrected for the spectral sensitivity of the spectrometer and diode-array detection system.

The luminescence spectra of the investigated fluorone dyes may have phosphorescence contributions in addition to the dominant fluorescence, i.e. the luminescence quantum yield is given by $\phi_L = \phi_F + \phi_P$. The phosphorescence contribution is approximately separated from the fluorescence contribution in the data analysis by plotting the luminescence spectra semi-logarithmically with linear wavelength scale and logarithmic luminescence quantum distribution scale. The fluorescence curves are then linearly extended to the long-wavelength region where a spectral overlap with the phosphorescence spectra occurs [45] (see Fig. 3, without the presence of phosophorescence generally an approximate long-wavelength exponential declining of the fluorescence signal is observed).

Fluorescence decay curves of the dye samples were measured by excitation with second harmonic pulses of a mode-locked Ti-

Table 1
Parameters of disodium fluorescein in different solvents (methanol with 0.1 mM NaOH).

Parameter	Gelatin	Starch	Chitosan	Methanol	Comments
$\lambda_{a,max}$ (nm)	502 ± 1	496 ± 1	502 ± 1	496 ± 1	Fig. 1
$\sigma_{a,max}$ (cm^2)	9.6×10^{-17}	1.0×10^{-16}	1.8×10^{-16}	2.2×10^{-16}	Fig. 2
$\Delta\nu_{abs}$ (cm^{-1})	2,673	2,486	1,773	1,452	Fig. 2
$\lambda_{F,max}$ (nm)	522 ± 1	519 ± 1	524 ± 1	520 ± 1	Fig. 3
$\Delta\nu_F$ (cm^{-1})	1,733	1,667	1,694	1,570	Fig. 3
ν_{01} (cm^{-1})	19,539	19,715	19,502	19,696	$(\lambda^{-1}_{a,max} + \lambda^{-1}_{F,max})/2$
$\delta\nu_{St}$ (cm^{-1})	763 ± 76	893 ± 78	836 ± 76	930 ± 78	$\lambda^{-1}_{a,max} - \lambda^{-1}_{F,max}$
ϕ_F	0.64 ± 0.03	0.71 ± 0.03	0.85 ± 0.04	0.97 ± 0.04	Fig. 3, Fig. 4
ϕ_P	≤0.003	≤0.005	≤0.001		Fig. 3
P_L	0.27 ± 0.02	0.19 ± 0.02	0.25 ± 0.03	0.04 ± 0.01	Fig. 8
τ_F (ns)	4.53 ± 0.03	5.05 ± 0.02	4.10 ± 0.04	5.49 ± 0.04	Fig. 5
τ_{rad} (ns)	7.1	7.1	4.8	5.6	$\tau_{rad} = \tau_F/\phi_F$

Abbreviations. $\lambda_{a,max}$: wavelength position of maximum S_0–S_1 absorption. $\sigma_{a,max}$: maximum S_0–S_1 absorption cross-section. $\Delta\nu_{abs}$ and $\Delta\nu_F$: spectral half-widths (FWHM) of first absorption and fluorescence bands, correspondingly. $\lambda_{F,max}$: wavelength position of maximum fluorescence emission. ν_{01}: wavenumber of pure electronic S_0–S_1 transition. $\delta\nu_{St}$: Stokes shift between S_0–S_1 absorption band and S_1–S_0 emission band. ϕ_F: fluorescence quantum yield. ϕ_P: phosphorescence quantum yield. P_L: degree of luminescence polarization. τ_F: fluorescence lifetime. τ_{rad}: radiative lifetime.

sapphire laser oscillator-amplifier system (laser system Hurricane from Spectra-Physics, excitation wavelength 400 nm, pulse duration 4 ps). The fluorescence emitted in backward direction was collected and directed to a micro-channel-plate photomultiplier (Hamamatsu type R1564-U01) through a broadband interference filter transmitting in the range from 500 to 610 nm. The photomultiplier signal was recorded with a fast digital oscilloscope (LeCroy type 9362).

3. Results

The absorption cross-section spectra of the investigated dyes in the applied biofilms and in basic methanol are displayed in Fig. 2. Relevant parameters as the wavelength position, $\lambda_{a,max}$, of peak S_0–S_1 absorption, the absorption cross-section, $\sigma_{a,max}$, at $\lambda_{a,max}$, and the spectral half-width, $\Delta\nu_F$, of the S_0–S_1 absorption band (FWHM) are collected in Tables 1–5 for the various dyes. With the exception of fluorescein and dibromofluorescein in starch the absorption bands are somewhat red-shifted compared to basic methanol. The spectral red-shift is a consequence of different solute–solvent interactions in the different hosts (depen-

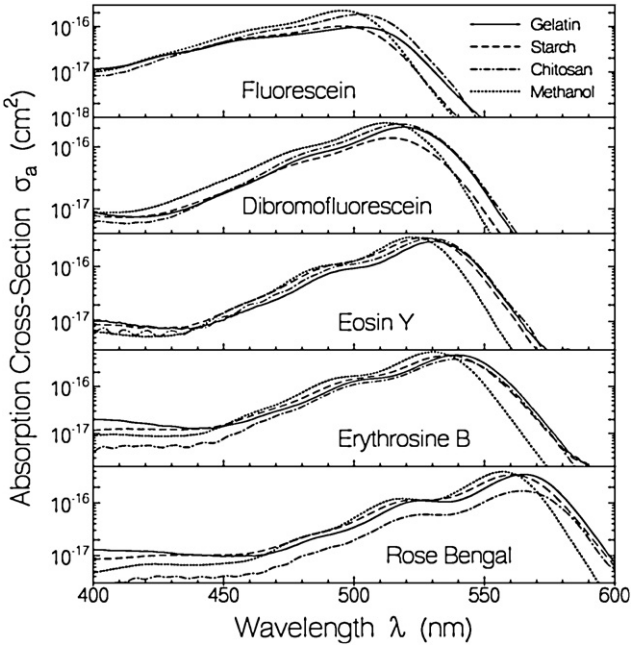

Fig. 2. Absorption cross-section spectra of investigated fluorone dyes.

Table 2
Parameters of dibromfluorescein in different solvents.

Parameter	Gelatin	Starch	Chitosan	Methanol
$\lambda_{a,max}$ (nm)	519 ± 1	514 ± 1	518 ± 1	513 ± 1
$\sigma_{a,max}$ (cm^2)	2.1×10^{-16}	1.4×10^{-16}	2.3×10^{-16}	2.4×10^{-16}
$\Delta\nu_{abs}$ (cm^{-1})	1,421	1,634	1,519	1,420
$\lambda_{F,max}$ (nm)	544 ± 1	541 ± 1	543 ± 1	539 ± 1
$\Delta\nu_F$ (cm^{-1})	1,570	1,726	1,644	1,613
ν_{01} (cm^{-1})	18,825	18,970	18,860	19,023
$\delta\nu_{St}$ (cm^{-1})	885 ± 71	970 ± 72	888 ± 71	940 ± 72
ϕ_F	0.55 ± 0.03	0.36 ± 0.02	0.57 ± 0.03	0.62 ± 0.03
ϕ_P	0.014 ± 0.01	≤ 0.009	0.011 ± 0.01	
P_L	0.19 ± 0.04	0.18 ± 0.03	0.21 ± 0.03	0.06 ± 0.01
τ_F (ns)	2.89 ± 0.02	2.49 ± 0.04	2.62 ± 0.03	3.46 ± 0.04
τ_{rad} (ns)	5.25	6.9	4.6	5.6

Table 3
Parameters of disodium eosin Y in different solvents.

Parameter	Gelatin	Starch	Chitosan	Methanol
$\lambda_{a,max}$ (nm)	531 ± 1	526 + 1	530 ± 1	523 ± 1
$\sigma_{a,max}$ (cm^2)	2.85×10^{-16}	3.35×10^{-16}	3.25×10^{-16}	3.45×10^{-16}
$\Delta\nu_{abs}$ (cm^{-1})	1,138	1,209	1,135	1,055
$\lambda_{F,max}$ (nm)	546 ± 1	545 ± 1	548 ± 1	544 ± 1
$\Delta\nu_F$ (cm^{-1})	1,468	1,603	1,537	1,355
ν_{01} (cm^{-1})	18,574	18,680	18,558	18,751
$\delta\nu_{St}$ (cm^{-1})	517 ± 69	662 ± 70	619 ± 70	738 ± 70
ϕ_F	0.60 ± 0.03	0.58 ± 0.03	0.61 ± 0.03	0.67 ± 0.03
ϕ_P	0.021 ± 0.01	0.019 ± 0.01	0.014 ± 0.01	
P_L	0.28 ± 0.03	0.21 ± 0.01	0.24 ± 0.06	0.07 ± 0.01
τ_F (ns)	2.91 ± 0.03	2.20 ± 0.04	2.39 ± 0.03	3.42 ± 0.04
τ_{rad} (ns)	4.85	3.8	3.9	5.1

Table 4
Parameters of disodium erythrosine B in different solvents.

Parameter	Gelatin	Starch	Chitosan	Methanol
$\lambda_{a,max}$ (nm)	539 ± 1	536 ± 1	539 ± 1	530 ± 1
$\sigma_{a,max}$ (cm^2)	4.7×10^{-16}	4.6×10^{-16}	3.8×10^{-16}	5.4×10^{-16}
$\Delta\nu_{abs}$ (cm^{-1})	1,072	1,160	1,137	1,023
$\lambda_{F,max}$ (nm)	554 ± 2	553 ± 2	558 ± 2	551 ± 2
$\Delta\nu_F$ (cm^{-1})	1,345	1,250	1,311	1,468
ν_{01} (cm^{-1})	18,468	18,370	18,237	18,508
$\delta\nu_{St}$ (cm^{-1})	502 ± 99	573 ± 100	631 ± 99	719 ± 101
ϕ_F	0.22 ± 0.02	0.13 ± 0.01	0.16 ± 0.01	0.13 ± 0.02
ϕ_P	0.071 ± 0.01	0.050 ± 0.01	0.049 ± 0.01	
P_L	0.37 ± 0.05	0.34 ± 0.02	0.34 ± 0.03	0.18 ± 0.02
τ_F (ns)	0.65 ± 0.05	0.35 ± 0.05	0.55 ± 0.05	0.45 ± 0.05
τ_{rad} (ns)	2.95	2.7	3.4	3.5

Table 5
Parameters of disodium rose bengal in different solvents.

Parameter	Gelatin	Starch	Chitosan	Methanol
$\lambda_{a,max}$ (nm)	565 ± 1	561 ± 1	565 ± 1	557 ± 1
$\sigma_{a,max}$ (cm^2)	3.5×10^{-16}	3.4×10^{-16}	1.7×10^{-16}	4.0×10^{-16}
$\Delta\nu_{abs}$ (cm^{-1})	902	1,012	1,060	870
$\lambda_{F,max}$ (nm)	578 ± 2	576 ± 2	576 ± 2	575 ± 3
$\Delta\nu_F$ (cm^{-1})	1,167	1,123	1,362	1,208
ν_{01} (cm^{-1})	17,500	17,593	17,530	17,672
$\delta\nu_{St}$ (cm^{-1})	398 ± 91	464 ± 92	338 ± 92	562 ± 123
ϕ_F	0.18 ± 0.01	0.09 ± 0.01	0.093 ± 0.02	0.10 ± 0.02
ϕ_P	0.013 ± 0.01	0.016 ± 0.01	0.006 ± 0.005	
P_L	0.39 ± 0.08	0.40 ± 0.01	0.37 ± 0.06	0.22 ± 0.03
τ_F (ns)	0.85 ± 0.05	0.45 ± 0.05	0.85 ± 0.05	0.60 ± 0.10
τ_{rad} (ns)	4.7	5.0	9.1	6.0

dent on dispersion force interaction, interaction of solute dipoles with induced solvent dipole moments, solute dipole–solvent dipole interaction, and solvent–dipole interaction with induced solute dipoles) [46,47]. In all cases a vibronic structure is resolved. The absorption spectra of the dyes shift to the red with increasing number and nuclear charge of halogens. The shift increases with the molar mass of the molecules.

Luminescence quantum distributions of the investigated samples are shown in Fig. 3. At the short wavelength side only fluorescence emission is present. At the long-wavelength side phosphorescence may contribute to the emission in the biofilms. The expected long-wavelength fluorescence emission for the dyes in gelatin is indicated by the dash-triple dotted curves. Parameters extracted from the luminescence curves are collected in Tables 1–5. These parameters are: the wavelength position of maximum fluorescence emission, $\lambda_{F,max}$, the spectral half-width of the fluorescence band (FWHM), $\Delta\nu_F$, the fluorescence quantum yield, $\phi_F = \int E_F(\lambda)\,d\lambda$, and the phosphorescence quantum yield, $\phi_P = \int E_L(\lambda)\,d\lambda - \phi_F$. The fluorescence spectra shift to longer wavelengths with the number of halogen atoms and the mass of the molecules. The fluorescence quantum yields of the investigated samples are visualized in Fig. 4. The fluorescence quantum efficiency reduces for the bromide substituted and more strongly for the iodide substituted fluorescein dyes (heavy atom effect). The fluorescence quantum yield of 4,5-dibromofluorescein is somewhat lower than the fluorescence quantum yield of 2,4,5,7-tetrabromofluorescein (eosin Y). This fluorescence quantum yield lowering is thought to be due to the use of 4,5-dibromofluorescein in hydrogenated form (R_4 = H) instead of disodium salt form (R_4 = Na, less basic solution lowering the fraction of dianionic dibromofluorescein). The effect of fluorescence quantum yield lowering is largest for 4,5-dibromofluorescein in starch.

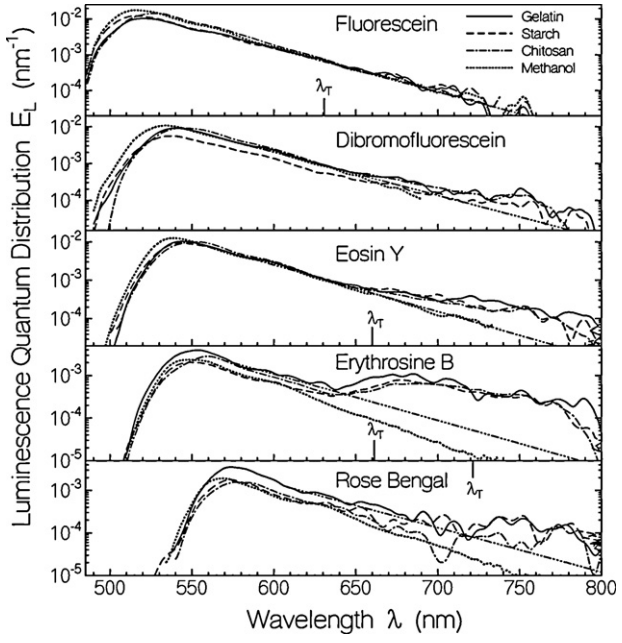

Fig. 3. Luminescence quantum distributions, $E_L(\lambda)$. Excitation wavelength was $\lambda_{ex,L}$ = 491 nm. Wavelength positions of phosphorescence maxima, λ_T, of dyes in ethanol at 77 K are included (from [48]). The dash-triple dotted lines are the linear fluorescence extensions for the dyes in gelatin.

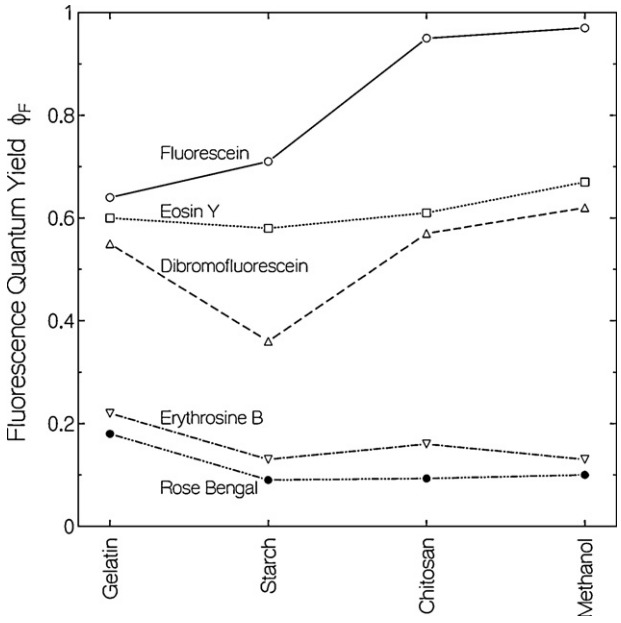

Fig. 4. Fluorescence quantum yields, ϕ_F, of investigated samples.

No phosphorescence emission was found for the fluorone dyes in the aerobic methanol solutions due to diffusion controlled oxygen quenching [28,29]. In the biofilms no phosphorescence was observed for fluorescein. A very weak phosphorescence may be present for dibromofluorescein in the biofilms. For eosin Y, erythrosine B, and rose bengal in the biofilms some phosphorescence was resolved. The phosphorescence is largest in the biofilms of erythrosine B. Higher phosphorescence emission would be expected at lower temperature where thermal activated non-radiative decays get frozen out.

The Stokes shift, $\delta\nu_{St}$, between the S_0–S_1 absorption and the S_1–S_0 emission transition is determined from the wavelength positions of maximum absorption and maximum emission. It is given by $\delta\nu_{St} = \nu_{a,max} - \nu_{F,max} = \lambda^{-1}_{a,max} - \lambda^{-1}_{F,max}$. The extracted values are included in Tables 1–5 and they are visualized in Fig. 5a. With the exception of erythrosine B, the Stokes shift is rather solvent independent. In erythrosine B a rising Stokes shift along gelatin, starch, chitosan, and methanol is observed.

The pure electronic S_0–S_1 transition frequencies, ν_{01}, are approximately given by $\nu_{01} = (\lambda^{-1}_{a,max} + \lambda^{-1}_{F,max})/2$. These transition frequencies are included in Tables 1–5 and visualized in Fig. 5b. They are rather independent of the solvent. The heavy atoms shift the transition frequencies to lower values (longer wavelengths).

Fluorescence decay curves of the studied dye samples are shown in Fig. 6a and b. Normalized curves, $S_F(t)/S_{F,max}$, are shown. The response function of the detection system is included (triple dotted curves). It was obtained by directing a strongly attenuated picosecond excitation laser pulse (second harmonic pulse of mode-locked Ti-sapphire laser) directly to the micro-channel-plate photomultiplier. In Fig. 6a fluorescence lifetimes are extracted from the fluorescence decay curves by single-exponential regression fits

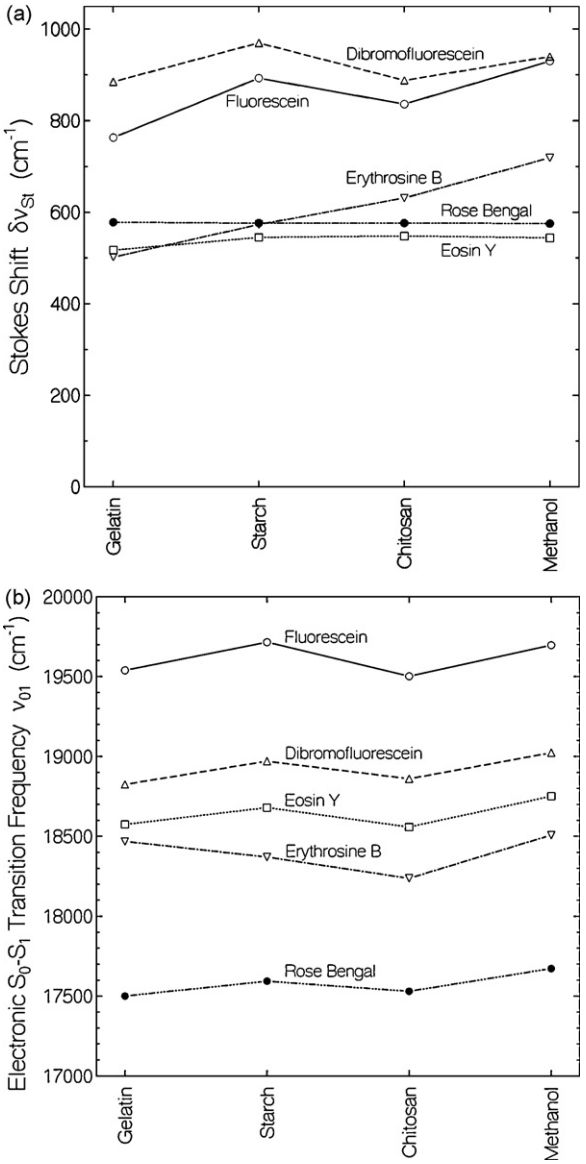

Fig. 5. (a) Stokes shifts between absorption and fluorescence maxima, $\delta\nu_{St}$, of investigated samples. (b) Electronic S_0–S_1 transition frequencies, ν_{01}, of investigated samples.

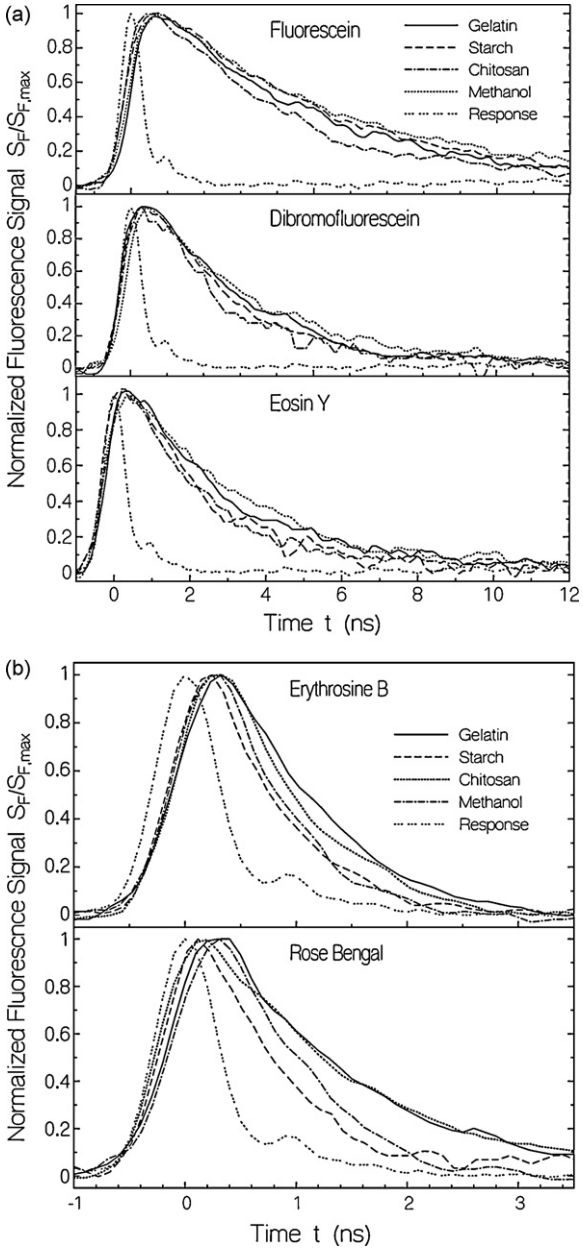

Fig. 6. (a and b) Fluorescence signal traces of investigated dyes. Response function of detection system is included.

$[S_F(t)/S_{F,max} = \exp(-t/\tau_F)]$. There the system response function (triple dotted curves) is short compared to the fluorescence decay times, τ_F, and therefore does not influence the determination of τ_F. For the fluorescence decay curves of Fig. 6b the finite width of the response function cannot be neglected. There the fluorescence lifetimes were extracted by curve de-convolution. The applied procedure is described in [49]. The determined fluorescence lifetimes are listed in Tables 1–5. The radiative lifetimes determined by $\tau_{rad} = \tau_F/\phi_F$ are also included in Tables 1–5. The fluorescence lifetimes are visualized in Fig. 7a. They are in the range of 4.4–5.5 ns for fluorescein, in the range of 2.4–3.4 ns for the bromine-substituted fluoresceins, and in the range of 350–850 ps for the iodine-substituted fluoresceins. No big difference is observed between 4,5-dibromofluorescein and 2,4,5,7-tetrabromofluoresein (eosin Y). The fluorescence lifetimes of erythrosine B are shorter than the fluorescence lifetimes of rose bengal for all studied hosts.

The radiative lifetimes are visualized in Fig. 7b. They decrease (absorption strength increases) with increasing molar mass (halogenation) of the dyes with the exception of rose bengal. 4,5-Dibromofluorescein in starch has a longer radiative lifetime (lower absorption strength) than in the other hosts. This may indicate that the ionicity of 4,5-dibromofluorescein in starch is shifted towards the neutral and single anionic form. For rose bengal the radiative lifetime in methanol and the biofilms is longer than expected. The chlorine ions on the carboxy-benzene ring seem to decrease the absorption strength of the xanthene core in comparison with erythrosine B. The long radiative lifetimes of rose bengal lead to longer fluorescence lifetimes for rose bengal compared to erythrosine despite the lower fluorescence quantum yield of rose bengal.

The degree of luminescence polarization, P_L, of the investigated dyes was determined by measuring the fluorescence spectra polarized parallel to the excitation light and perpendicular to the excitation light as described above (Eq. (2)). For isotropic samples in the ground-state before excitation the degree of luminescence polarization may vary between $P_L = 0$ in the case of infinitely fast

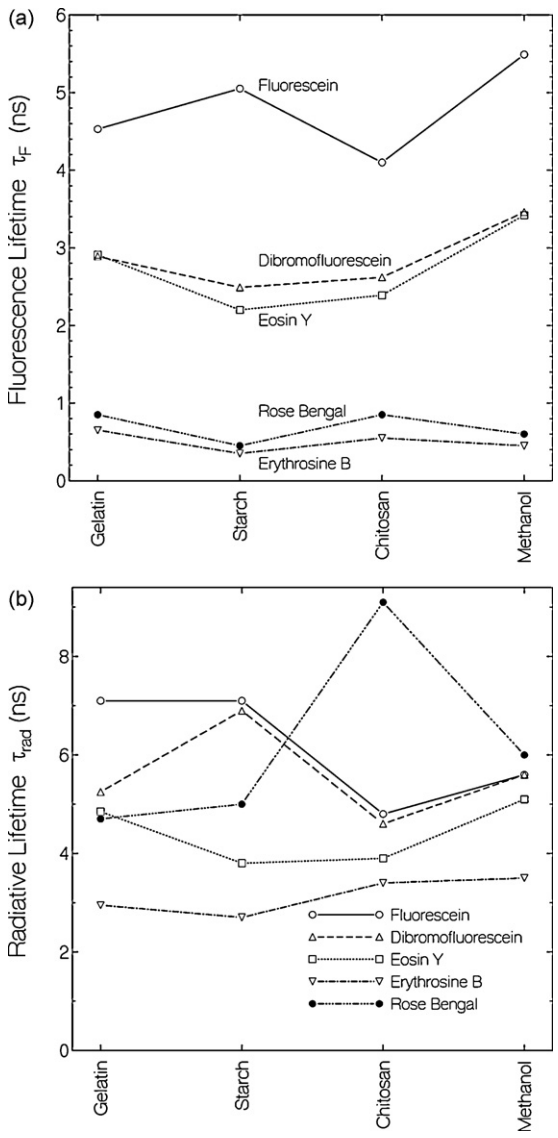

Fig. 7. (a) Fluorescence lifetimes, τ_F, of investigated samples. (b) Radiative lifetimes, τ_{rad}, of investigated samples.

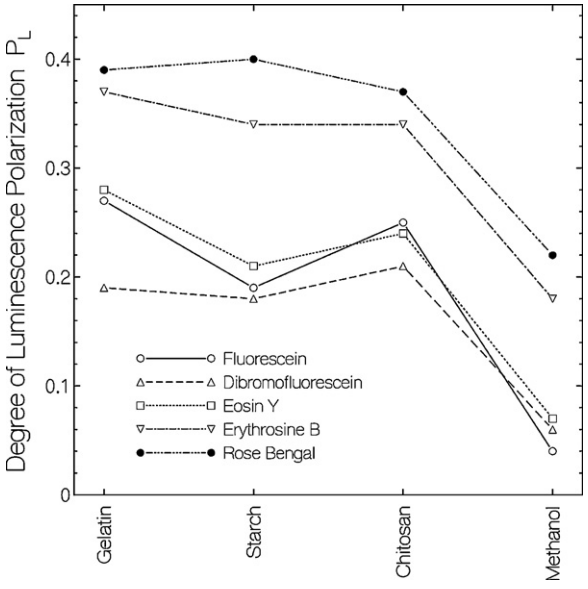

Fig. 8. Degree of luminescence polarization, P_L, of investigated samples.

reorientation of the transition dipole moments and $P_L = 0.5$ in the case of parallel orientation of absorption and emission transition dipole moments and no reorientation within the excited state lifetime [50]. The obtained results are included in Tables 1–5 and they are visualized in Fig. 8. In the biofilms moderately high degrees of fluorescence polarization were obtained since molecular reorientation within the fluorescence lifetime is inhibited by the solid matrix (no molecular reorientation). Some reorientation of the transition dipole moments occurs due to excitation energy transfer between excited and unexcited molecules [51,52]. Asymmetric vibrational mode excitation and molecular symmetry (no sharp orientation of transition dipole moments) may contribute to luminescence depolarization [53]. The degree of fluorescence polarization is highest for erythrosine B and rose bengal because of the short fluorescence lifetime. In methanol the degree of luminescence polarization was found to be small because of molecular reorientation in the low-viscous fluid within the luminescence lifetime (largest values for erythrosine B and rose bengal because of short fluorescence lifetimes).

4. Discussion

4.1. Protolytic versatility of fluorescein and its derivatives

Depending on the solvent acidity or basicity the fluorone dyes exist in different ionic states with different absorption and emission behavior [54–58]. The different cationic, zwitter-ionic, neutral, lactonic, anionic, and dianionic forms are depicted in Fig. 9 (from [55]). In aqueous solution the ionic state changes with pH. For fluorescein and dibromofluorescein the pK values for the equilibrium conditions of the various forms have been determined in [57]. The reported values are $pK_{a,0} = 0.94$ for the acid–neutral equilibrium, $pK_{a,1} = 6.82$ for the neutral–anionic equilibrium, and $pK_{a,2} = 7.66$ for the anionic–dianionic equilibrium of fluorescein. The corresponding parameters for dibromofluorescein are $pK_{a,1} = 5.85$ and $pK_{a,2} = 6.24$. The fluorescence efficiency was found to depend on the ionicity of the fluorone dyes [58]. In the case of fluorescein weak fluorescence was found for the cationic form, practically no fluorescence was found for the neutral form; for the single-anionic form a fluorescence quantum yield of $\phi_F = 0.37$ was determined, and for the dianionic form a fluorescence quantum yield of $\phi_F = 0.93$ was measured. In our experiments presented above we used methanol containing 0.1 mM NaOH to shift the ionicity of the studied fluorone dyes towards the dianionic form. In additional studies on fluorescein (4,5-dibromofluorescein) in neutral methanol we obtained luminescence quantum yields of $\phi_F = 0.75 \pm 0.04$ (0.61 ± 0.03), and for fluorescein (4,5-dibromofluorescein) in methanol containing 0.1 mM HCl we determined $\phi_F = 0.53 \pm 0.03$ (0.12 ± 0.02). For eosin Y, erythrosine B, and rose bengal in neutral methanol and methanol with 0.1 mM HCl we determined the same fluorescence quantum yield as for methanol with 0.1 mM NaOH within our experimental accuracy indicating the dominance of dianionic forms in these cases.

In the biofilms, the ionic state of the fluorone dyes may be guessed from the fluorescence efficiency. In chitosan the fluorescence quantum yield of fluorescein is nearly as high as in basic methanol indicating the dominant presence of fluorescein in dianionic form. In starch and gelatin the fluorescence efficiency of fluorescein is reduced indicating the dominant presence of fluorescein in the single-anionic form. 4,5-Dibromofluorescein in chitosan and gelatin is thought to be present in dianionic form, while in starch the lowered fluorescence efficiency and longer radiative lifetime indicates the presence of some amount of single-anionic and neutral form. Eosin Y, erythrosine B, and rose bengal seem to be present in dianionic form. The fluorescence quantum yield gets dominantly determined by the heavy atom effect.

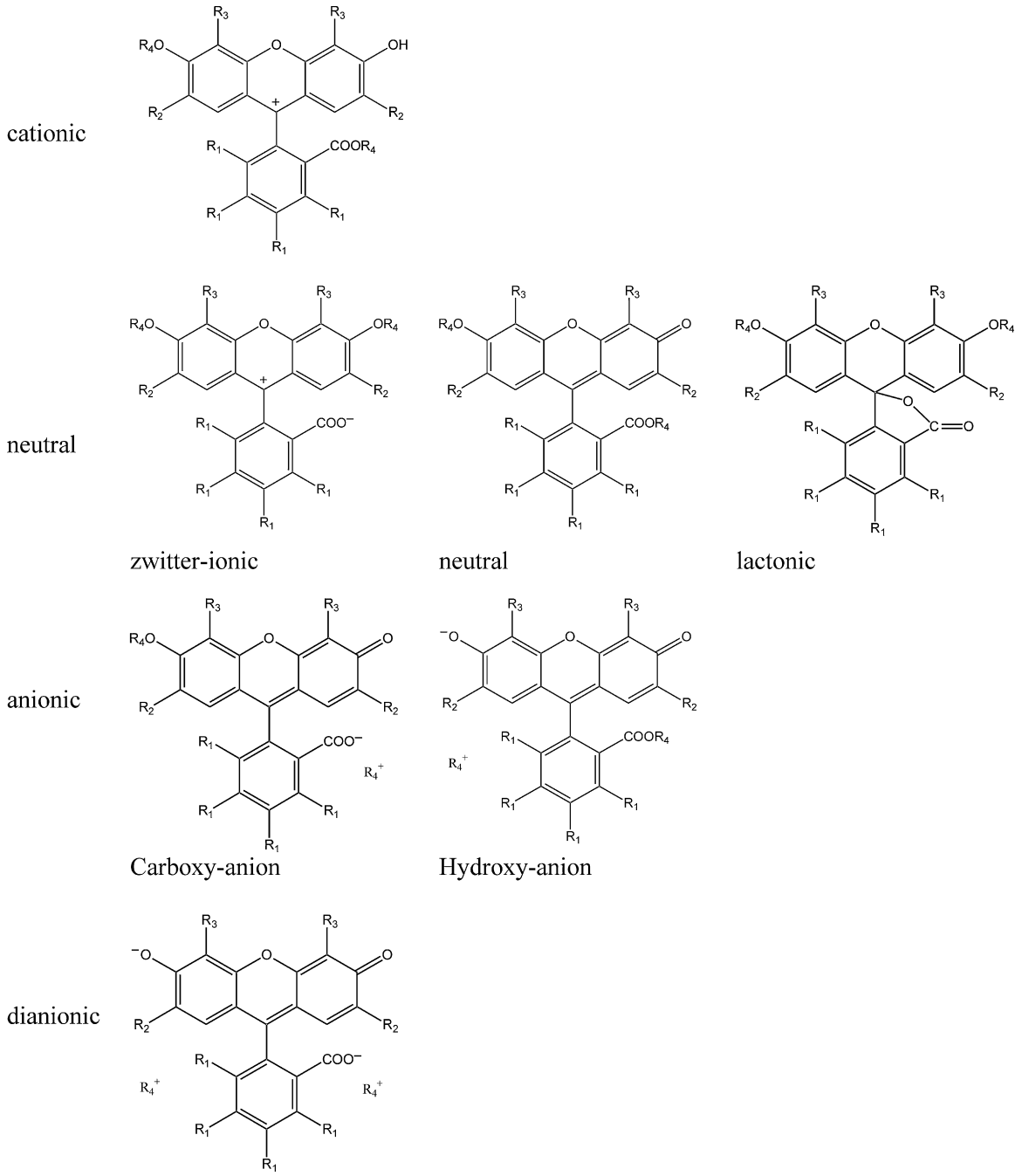

Fig. 9. Ionic and molecular forms of fluorone dyes (after [57]).

4.2. Spin-orbit coupling (triplet formation) by bromine and iodine substituent atoms

The fluorescence lifetime (and consequently the fluorescence quantum yield) of the investigated fluorone dyes decreased with bromine substitution and more severely with iodine substitution. This effect is due to enhancement of singlet-triplet intersystem-crossing (enhancement of excited-state triplet formation) by heavy atom spin-orbit coupling [59,60]. The heavy substituent atoms perturb the π-electron state of the dye molecules, resulting in a mixing of the triplet and singlet states. The strength of the coupling is governed by the atomic spin-orbit coupling factor ζ_k of the substituent k. The contribution to the rate of intersystem crossing is expected to be proportional to ζ_k^2 [27,60,61]. ζ_k values are listed in [62]. They are $\zeta_{Br} = 2450\,cm^{-1}$ and $\zeta_I = 5250\,cm^{-1}$.

Quantum yields of triplet formation, ϕ_{S_1,T_1}, were determined in [25,63]. Reported values are ϕ_{S_1,T_1} (fluorescein in ethanol) = 0.03 [63], ϕ_{S_1,T_1} (dibromofluorescein in ethanol) = 0.33 [63], ϕ_{S_1,T_1} (eosin Y in methanol) = 0. [25], ϕ_{S_1,T_1} (erythrosine B in methanol) = 0.58 [25], and ϕ_{S_1,T_1} (rose bengal in methanol) = 0.52 [25]. The rates of intersystem crossing are given by $k_{S_1,T_1} = \phi_{S_1,T_1}/\tau_F$. Using the measured τ_F values of this paper we calculate k_{S_1,T_1} (fluorescein) = $5.5 \times 10^6\,s^{-1}$, k_{S_1,T_1} (dibromofluorescein) = $9.5 \times 10^7\,s^{-1}$, k_{S_1,T_1} (eosin Y) = $7.3 \times 10^7\,s^{-1}$, k_{S_1,T_1} (erythrosine B) = $1.3 \times 10^9\,s^{-1}$, and k_{S_1,T_1} (rose bengal) = $8.7 \times 10^8\,s^{-1}$. The ratio of the intersystem crossing rates is k_{S_1,T_1}(fluorescein) : k_{S_1,T_1}(dibromofluorescein) : k_{S_1,T_1}(eosin Y) : k_{S_1,T_1}(erythrosine B) : k_{S_1,T_1}(rose bengal) = 0.058 : 1 : 0.77 : 18 : 12. The ratio of the sum of squares of the spin-orbit coupling factors is $2\zeta_{Br}^2$(dibromofluorecein) : $4\zeta_{Br}^2$(eosin Y) : $4\zeta_{Br}^2$(erythrosine B) : $4\zeta_{Br}^2$(rose bengal) = 1 : 2 : 9.2 : 9.2. This

comparison shows the enhancement of intersystem-crossing with the heavy atom mass and some dependence on the specific location and mutual interaction of the heavy atoms. The chlorine atoms on the carboxy-benzene ring of rose bengal seems to lower somewhat the rate of intersystem crossing.

4.3. Comparison of fluorone dyes in biofilms and methanol

Comparative spectroscopic studies on the fluorone dyes in biofilms and methanol were undertaken to get knowledge about the absorption and emission behavior of these dyes in polypeptides (gelatin protein), polysaccharides (starch), and polyaminosaccharides (chitosan). The knowledge of this spectroscopic behavior is a prerequisite in the application of these fluorone dyes in bio-labeling, biofilm sensing, and biofilm device development.

In the biofilms the S_0–S_1 absorption band of the fluorone dyes is red-shifted compared to basic methanol with the exception of fluorescein and 4,5-dibromofluorescein in starch. The absorption strength of fluorescein in starch, 4,5-dibromofluorescein in starch, and rose bengal in chitosan is lowered compared to the other hosts and basic methanol solvent. The changes are thought to be caused by changes of the ionicity of the dyes in the hosts. A lowering of absorption strength was observed for the studied fluorone dyes in acidic methanol where the ionicity changed to single anionic and neutral forms.

The shapes of the fluorescence spectra in the biofilms and in basic methanol are rather similar. Phosphorescence emission was observed for eosin Y, erythrosine B, and rose bengal in the biofilms at room temperature. Most efficient phosphorescence emission occurred for erythrosine B. In the aerobic methanol solutions no phosphorescence was observed because of diffusion controlled triplet state quenching by the dissolved oxygen.

The fluorescence lifetimes are not strongly different in basic methanol solution and in the biofilms. The lifetime is strongly influenced by the atoms in the 4 and 5 position of the xanthene core. The heavy atom fluorescence quenching by intersystem-crossing is approximately the same for 4,5-dibromofluorescein and 2,4,5,7-tetrabromofluorescein (eosin Y) on one side and for erythrosine B and rose bengal on the other side.

The degree of fluorescence polarization shows the expected viscosity and fluorescence lifetime dependence: it is higher in solid matrix than in solution since molecular reorientation is inhibited, and it rises with decreasing fluorescence lifetime since the action time of transition dipole moment reorientation is shortened.

5. Conclusions

The absorption and emission spectroscopic behavior of fluorescein, dibromine fluorescein, tetrabromine fluorescein, tetraiodine fluorescein and tetrachlorine–tetraiodine fluorescein in protein films (gelatin), polysaccharide films (starch), polyaminosaccharide films (chitosan) and methanol solution was studied. The fluorone dye behavior in liquid solutions is generally dependent on the solvent ionicity causing absorption and emission changes with basic, neutral, and acid solvent nature. Observed host dependencies in the biofilms are likely due to ionicity changes of the fluorone dyes in the different hosts. The intramolecular heavy atom fluorescence reduction by enhanced intersystem crossing is acting both in the biofilms and in methanol. No protein, polysaccharide, or polyaminosaccharide specific fluorescence quenching by photo-induced external electron transfer or proton transfer was observed. The performed studies may give valuable information for the application of the fluorone dyes in photo-biological applications.

Acknowledgments

One of the authors, E. Slyusareva, gratefully acknowledges the support by the Deutsche Akademischer Austausch Dienst (DAAD) and the Education Ministry of Russian Federation for providing her a fellowship ("Michail Lomonosov" program). The authors thank M. Gerasimova for helpful information.

References

[1] F.P. Schäfer (Ed.), Dye Lasers, Springer, Berlin, 1990.
[2] F.J. Duarte, L.W. Hillman (Eds.), Dye Laser Principles with Applications, Academic Press, San Diego, 1990.
[3] M. Maeda, Dyes. Laser, Properties of Organic Compounds for Dye Lasers, Academic Press, San Diego, 1984.
[4] P.E. Tverdokhleb (Ed.), 3D Laser Information Technologies, Institute of Automatics and Electrometry of SB RAS, Novosibirsk, 2003.
[5] I.D. Johson, in: J.B. Pawley (Ed.), Handbook of Biological Confocal Microscopy, third ed., Springer Science + Business Media, LLC, New York, 2006, pp. 353–367.
[6] R.P. Haugland, Handbook of Fluorescent Probes and Research Products, ninth ed., Molecular Probes, Inc., Eugene, OR, USA, 2002.
[7] J.R. Lakowicz, Principles of Fluorescence Spectroscopy, third ed., Springer, New York, 2006.
[8] T. Hirano, K. Kikuchi, Y. Urano, T. Nagano, Improvement and biological applications of fluorescent probes for Zinc, ZnAFs, J. Am. Chem. Soc. 124 (2002) 6555–16555.
[9] Dong-Hui Li, Quing-Zhi Zhu, Dong Ye, Ying Fang, Jin-Gou Xu, A rapid method for determination of molar ratio of fluorofore to protein by fluorescence anisotropy detection, Anal. Chim. Acta 389 (1999) 85–88.
[10] X. Guan, X. Liu, Z. Su, Preparation and photophysical behaviors of fluorescent chitosan bearing fluorescein: potential biomaterial as temperature/pH probes, J. Appl. Polym. Sci. 104 (2007) 3960–3966.
[11] C.-A. Chen, R.-H. Yeh, D.S. Lawrence, Design and synthesis of a fluorescent reporter of protein kinase activity, J. Am. Chem. Soc. 124 (2002) 3840–3841.
[12] D. Madge, R. Wong, P.G. Seybold, Fluorescence quantum yields and their relation to lifetimes of rhodamine 6G and fluorescein in nine solvents: improved absolute standards for quantum yields, Photochem. Photobiol. 75 (2002) 327–334.
[13] A. Birla, M. Cristian, Hillebrand, Absorption and steady state fluorescence study of interaction between eosin and serum albumin, Spectrochim. Acta Part A 60 (2004) 551–556.
[14] M.D. Lyman, D. Melanson, A.S. Sawhney, Characterization of the formation of interfacially photopolymerized thin hydrogels in contact with arterial tissue, Biomaterials 17 (1996) 359–364.
[15] S.K. Lam, M.A. Chan, D. Lo, Characterisation of phosphorescence oxygen sensor based on erythrosine B in sol–gel silica in wide pressure and temperature ranges, Sens. Actuators B 73 (2001) 135–141.
[16] A.G. Sizykh, E.A. Tarakanova, Photoinduced processes in solid polymer solution of a dye in interference field of laser radiation, Quant. Electron. 28 (1998) 1097–1101.
[17] A.G. Sizykh, E.A. Tarakanova, L.L. Tatarinova, Laser-induced reduction of a dye characterized by a high triplet state yield and dissolved in polymer, Quant. Electron. 30 (2000) 40–44.
[18] A.G. Sizykh, E.A. Slyusareva, Application of light-induced gratings for measurement of laser irradiation characteristics, Izvestiya Vuzov. Fizika 51 (2008) 74–79.
[19] M. Martin, Hydrogen bond effects on radiationless electronic transition in xanthene dyes, Chem. Phys. Lett. 35 (1975) 105–111.
[20] G.R. Fleming, A.W.E. Knight, J.M. Morris, R.J.S. Morrison, G.W. Robinson, Picosecond fluorescence studies of xanthene dyes, J. Am. Chem. Soc. 99 (1977) 4306–4311.
[21] N.B. Joshi, P. Gangola, D.D. Pant, Internal heavy atom effect on the radiative and non-radiative rate constants in xanthene dyes, J. Luminesc. 21 (1979) 111–118.
[22] N.B. Joshi, D.D. Pant, Effect of aggregation on the radiative ($T_1 \rightarrow S_0$) and non-radiative ($T_1 \rightsquigarrow S_0$ and $S_1 \rightsquigarrow T_1$) transitions in xanthene dyes, J. Luminesc. 14 (1976) 1–8.
[23] H. Gratz, A. Penzkofer, Triplet–triplet absorption of some organic molecules determined by picosecond laser excitation and time delayed picosecond light continuum probing, J. Photochem. Photobiol. A: Chem. 127 (1999) 21–30.
[24] A. Penzkofer, A. Beidoun, M. Daiber, Intersystem-crossing and excited-state absorption in eosin Y solutions determined by picosecond double pulse transient absorption measurements, J. Luminesc. 51 (1992) 297–314.
[25] S. Reindl, A. Penzkofer, Higher excited-state triplet–singlet intersystem crossing of some organic dyes, Chem. Phys. 213 (1996) 429–438.
[26] S.K. Lam, D. Lo, Time resolved spectroscopic study of phosphorescence and delayed fluorescence of dyes in silica-gel glasses, Chem. Phys. Lett. 281 (1997) 35–43.
[27] M.P. Lettinga, H. Zuilhof, M.A.M.J. van Zandvoort, Phosphorescence and fluorescence characterization of fluorescein derivatives immobilized in various polymer matrices, Phys. Chem. Chem. Phys. 2 (2000) 3697–3707.
[28] P.B. Garland, C.H. Moore, Phosphorescence of protein-bound eosin and erythrosine. A possible probe for measurements of slow rotational mobility, Biochem. J. 183 (1979) 561–572.

[29] R. Duchowicz, M.L. Ferrer, A.U. Acuña, Kinetic spectroscopy of erythrosine phosphorescence and delayed fluorescence in aqueous solution at room temperature, Photochem. Photobiol. 68 (1998) 494–501.
[30] Y. Silberberg, I. Bar-Joseph, Low power phase conjugation in thin films of saturable absorbers, Opt. Commun. 39 (1981) 265–268.
[31] M.A. Kramer, W.R. Tompkin, R.W. Boyd, Nonlinear-optical interactions in fluorescein-doped boric acid glass, Phys. Rev. A 34 (1986) 2026–2031.
[32] W.R. Tompkin, M.S. Malcuit, R.W. Boyd, Enhancement of the nonlinear optical properties of fluorescein doped boric-acid glass through cooling, Appl. Opt. 29 (1990) 3921–3926.
[33] R.A.A. Muzzarelli (Ed.), Chitosan per os: From Dietary Supplement to Drug Carrier, Atec, Grottammare, 2000.
[34] K.G. Skryabin, G.A. Vihoreva, V.P. Varlamova (Eds.), Chitin and Chitosan: Production, Properties and Application, Nauka, Moskva, 2002.
[35] P.J. VandeVord, H.W.T. Matthew, S.P. DeSilva, L. Mayton, B. Wu, P.H. Wooley, Evaluation of the biocompatibility of a chitosan scaffold in mice, J. Biomed. Mater. Res. 59 (2002) 505–590.
[36] X. Qu, A. Wirsén, A.-C. Albertsson, Novel pH-sensitive chitosan hydrogels: swelling behavior and states of water, Polymer 41 (2000) 4589–4598.
[37] V. Kratasyuk, E. Esimbekova, Polymer immobilized bioluminescent systems for biosensors and bioinvestigations, in: R. Arshady (Ed.), Polymeric Biomaterials, the PBM Series, vol. 1, Citus Books, London, 2003, pp. 301–343.
[38] S.J. Strickler, R.A. Berg, Relationship between absorption intensity and fluorescence lifetime of molecules, J. Chem. Phys. 37 (1962) 814–822.
[39] J.B. Birks, D.J. Dyson, The relations between the fluorescence and absorption properties of organic molecules, Proc. Roy. Soc. Lond., Ser. A 275 (1963) 135–148.
[40] A.V. Deshpande, A. Beidoun, A. Penzkofer, G. Wagenblast, Absorption and emission spectroscopic investigation of cyanovinyldiethylaniline dye vapors, Chem. Phys. 142 (1990) 123–131.
[41] A. Penzkofer, W. Leupacher, Fluorescence behaviour of highly concentrated rhodamine 6G solutions, J. Luminesc. 37 (1987) 61–72.
[42] W. Holzer, M. Pichlmaier, A. Penzkofer, D.D.C. Bradley, W.J. Blau, Fluorescence spectroscopic behaviour of neat and blended conjugated polymer thin films, Chem. Phys. 246 (1999) 445–462.
[43] Th. Förster, Fluoreszenz organischer Verbindungen, Vandenhoeck and Ruprecht, Göttingen, 1951.
[44] R. Sens, Strahlungslose Desaktivierung in Xanthen, Oxazin und Carbazinfarbstoffen, Dissertation, Universität-Gesamthochschule Siegen, Siegen, 1984.
[45] T. Tsuboi, A.K. Bansal, A. Penzkofer, Temperature dependence of fluorescence and phosphorescence of the triphenylamine dimer 3-methyl-TPD, Opt. Mater. 31 (2009) 980–988.
[46] M. Mataga, T. Kubato, Molecular Interaction and Electronic Spectra, Dekker, New York, 1970.
[47] A.V. Deshpande, A. Beidoun, A. Penzkofer, G. Wagenblast, Spectroscopic investigation of cyanovinyl-diethylaniline dyes in solutions, Chem. Phys. 148 (1990) 141–154.
[48] Sh.D.M. Islam, T. Susdorf, A. Penzkofer, P. Hegemann, Fluorescence quenching of flavin adenine dinucleotide in aqueous solution by pH dependent isomerisation and photo-induced electron transfer, Chem. Phys. 295 (2003) 137–149.
[49] F. Dörr, Spectroscopy with polarised light, Angew. Chem. Internat. Ed. 5 (1966) 478–495.
[50] V.L. Ermolaev, E.N. Bodunov, E.B. Sveshnikova, T.A. Shahverdov, Nonradiative Energy Transfer of Electron Excitation Energy, Nauka, Leningrad, 1977.
[51] A. Ore, Intermolecular energy transfer and concentration depolarization of fluorescent light, J. Chem. Phys. 31 (1959) 442–443.
[52] A. Penzkofer, W. Falkenstein, Photoinduced dichroism and vibronic relaxation of rhodamine dyes, Chem. Phys. Lett. 44 (1976) 547–552.
[53] R. Markuszewski, H. Diehl, The infrared spectra and structures of the three solid forms of fluorescein and related compounds, Talanta 27 (1980) 937–946.
[54] J. Paczkowski, J.J.M. Lamberts, B. Paczowska, D.C. Neckers, Photophysical properties of rose bengal and its derivatives (XII), J. Free Rad. Biol. Med. 1 (1985) 341–351.
[55] D.C. Neckers, O.M. Valdes-Aguilera, The photochemistry of the xanthene dyes, Adv. Photochem. 18 (1993) 315–394.
[56] N.O. Mchedlov-Petrosyan, N.A. Vodlazkaya, V.P. Martynova, D.V. Samoiov, A.V. El'tsov, Protolytic properties of thiofluorescein and its derivatives, Russ. J. Gen. Chem. 72 (2002) 785–792.
[57] R. Sjöback, J. Nigren, M. Kubista, Absorption and fluorescence properties of fluorescein, Spectrochim. Acta, Part A 51 (1995) L7–L21.
[58] D.S. McClure, Triplet–singlet transitions in organic molecules. Lifetime measurements of the triplet state, J. Chem. Phys. 17 (1949) 905–913.
[59] S.P. McGlynn, T. Azumi, M. Kinoshita, Molecular Spectroscopy of Triplet State, Prentice–Hall, Englewood Cliffs, New Jersey, 1969.
[60] M. Zander, G. Kirsch, On the phosphorescence of benzologues of furan, thiophene, selenophene, and tellurophene. A systematic study of the intra-annular internal heavy-atom effect, Z. Naturforschung 44a (1989) 205–209.
[61] N.J. Turro, Molecular Photochemistry, W.A. Benjamin, Inc., New York, 1978.
[62] E. Gandin, Y. Lion, A. Van de Vorst, Quantum yield of singlet oxygen production by xanthene derivatives, Photochem. Photobiol. 37 (1983) 271–278.
[63] K. Gollnick, T. Franken, M.F.R. Fouda, H.R. Paur, S. Held, Merbromin (mercurochrome) and other xanthene dyes: quantum yields of triplet sensitizer generation and singlet oxygen formation in alcoholic solutions, J. Photochem. Photobiol. B: Biol. 12 (1992) 57–81.